ZANCO Journal of Pure and Applied Sciences

TYPE Original Research
DOI http://dx.doi.org/10.21271/ZJPAS.36.4.3

OPEN ACCESS

*Corresponding author

Ahmed H. Kurda
ahmed.kurda@su.edu.krd

RECEIVED :23 /09 2023
ACCEPTED :02/05/ 2024
PUBLISHED :31/ 08/ 2024

KEYWORDS:

ZnO Nanostructure, SILAR Procedure, Planar Photodetector, Silicon, Porous Silicon, Responsivity, and Sensitivity.

Photodetector Devices: Investigation of ZnO Thin Films Fabricated via SILAR Technique on Various Substrates:

Shaida Anwar Kakil[1] ,Ahmed HassanKurda[1], Yousif Mawlood Hassan[1]

1Department of Physics, College of Science, Salahaddin University-Erbil, Erbil, Kurdistan Regine, Iraq.

ABSTRACT

The synthesis of photodetectors for ZnO nanostructure films on various substrates, including p-type (100) silicon (Si), and porous silicon (pSi), has been achieved through the utilization of a straightforward technique known as the successive ionic layer adsorption and reaction (SILAR) method. To analyze the optical properties, surface morphology, and crystal structure of the ZnO layers, UV-Vis spectrometers, field emission scanning electron microscopes (FESEM), and X-ray diffraction (XRD) were employed. The characterization of the ZnO samples revealed that the number of SILAR cycles has a significant impact on the morphology and optical band gap of the synthesized layer. The Fourier-transform infrared (FTIR) spectrum successfully detected the distinctive extended vibration mode of ZnO. By conducting 20 cycles, high-quality hexagonal ZnO was obtained. The responsivity of the planar ZnO on silicon (ZnO/Si) and ZnO on the porous silicon (ZnO/pSi) surface exhibited variations depending on the substrate surface and bias voltage. The results indicated that the (ZnO/pSi) heterojunction demonstrated a high response in the visible range (350–850 nm) at a low bias voltage. On the other hand, the (ZnO/Si) photodetector displayed a high sensitivity of 666.66% at a low voltage of 1V in comparison to the (ZnO/pSi) photodetector, which exhibited a sensitivity of 483%.

1. Introduction

In recent times, due to its extensive commercial and technological application, the photodetection device has garnered significant attention. All applications require very sensitive devices with rapid response speed. There are various types of detectors available, with Si-based photodetectors and photomultipliers being the most common ones (Bayan, 2024). These devices exhibit exceptional sensitivity in the light spectrum, along with low noise and quick response. Owing to its extensive bandgap, affordability, robust radiation stiffness, and in-height chemical stability (Wisz et al., 2017; Jiang et al., 2023), is considered a highly promising candidate for manufacturing ultraviolet radiation detectors (Khokhra, et al., 2017; Boruah, 2019), high-temperature lighting diodes (Rahman, 2019; Rahman et al., 2023) and visible-UV photo-detection, (Guo, et al., 2020; Zhang, et al., 2020). Laser diodes (Lu, et al., 2019; Al-Heuseen, Aljameel, and Hussein, 2024). ZnO thin nanostructure films were precipitated by various techniques, including spray pyrolysis (Al-Rasheedi, et al., 2022), sol-gel (Al Abdullah et al., 2017) pulsed laser deposition (Nikov, et al., 2017), chemical bath deposition (More, et al., 2023), electrodeposition (Syrek, et al., 2023), successive ionic layer adsorption and reaction (SILAR) (Cruz, et al., 2018; Sreedev, et al., 2019; Ghos et al., 2021;). The SILAR technique is a simple solution process that does not need any complicated tools. In SILAR technology, the metal ion is adsorbed on the base surface as a solitary film, and then the compact film is shaped to do the chemical response with the adhesion ion and the hydrolysis of the ions (Govender, et al., 2014). For some reason, substrate surfaces might affect the construction, optical properties, and convenience of large-scale deposited films.

Nowadays, porous silicon has attracted a lot of attention due to its important optical properties. We know that crystalline silicon has an indirect gap of 1.1eV at room temperature. This leads to a very ineffective radiological absorption in the near-infrared spectrum. Therefore, the strong visible light absorption in porous silicon is quite surprising and such a structure can appear in a large variety of shapes and particle sizes. It is not easy to deposit a large area and high uniformity of ZnO nanocrystals on the polished Si substrates because of the large mismatch in thermal coefficient and lattice constant (Tripathy, et al., 2018). The growing of ZnO nanocrystals by the SILAR method is the lowest-top approach and the morphology of the base surface is an important factor in obtaining high-quality nanocrystal films. Our results agree with Shabannia and Naderi (Shabannia, and Naderi, 2019); they prepared high-density ZnO on a porous surface using the chemical bath deposition technique.

However, according to previous researchers, the direct growth or deposition of high-quality ZnO on Si substrates was found to be difficult (Wang, et al.,2012; Xu, et al., 2015). To overcome these problems, some surface pre-treatment techniques such as the pours of suffuses. The porous silicon (PS) is an intensively studied material, which has characteristics of high resistance, large internal surface, and strong absorbability (Shaoqiang, et al., 2004).

In our research, the strong absorbability of PS was a benefit to us since it was believed that the bonding of ZnO on Si substrate could be enhanced by the increased surface area. Another important property of porous silicon is its superior optoelectronic characteristic. Hence, it is believed that the combination of ZnO films and pours silicon substrate will overcome the problems mentioned above and lead to a new type of potential functional material.

In this work, ZnO nanostructures have been done by a modest, low-cost SILAR technique with various cycles of deposition on silicon and pour silicon. Substrates formed by electrochemical etching technology. The Planar (ZnO/Si), and (ZnO/pSi) heterojunction photodetectors were manufactured and analyzed. Here we established a high-performance wide-band photodetector based on a (ZnO/pSi) heterojunction assembly.

2. Methodology

2.1 Synthesis of porous silicon nanostructure

Porous silicon nanostructures were fabricated electrochemically using a boron-doped Si (100) wafer. The deposition process employed a Teflon container, with the Si wafer serving as the anode and the Platinum wire as the cathode. The

electrolyte consisted of a mixture of (Hydrofluoric acid, HF (49%), and (Ethanol (95%), at a ratio of 1:4. A current with a density of 25 mA/cm^2 was applied for 3 minutes. Following the electrochemical process, the specimens underwent a washing procedure using water deionized (DI) and were subsequently dried using a hairdryer.

2.2 Growth ZnO on Si and pSi

The ZnO nanostructure was synthesized on a glass p-type Si, and pSi base via the SILAR procedure. Through utilizing 29% ammonium hydroxide (NH_4OH, Merck Co. Germany) and 0.1M zinc chloride ($ZnCl_2$, 99.7%, Merck Co. Germany). To bring the pH of the zinc composite ($[Zn(NH_3)4]^{2+}$) solution down to roughly 10 ammonium hydroxide was used. Zn (OH) was changed into ZnO propylene glycol at 100℃. The following steps were taken to deposit ZnO films on the bases: Immersion 1: For 20 seconds, the bases were submerged in zinc ammonia composite $[Zn(NH_3)_4]^{2+}$ to allow $Zn(OH)_2$ to precipitate on the bases and adsorbed on the base surface. Immersion 2: For 30 seconds, surface. The bases were submerged in hot deionized water to evacuate the ions that were adhered to the $Zn(OH)_2$ grains from the surface. Immersion 3: ZnO formed on the bases after they were submerged in propylene glycol for 20 seconds at 100℃. Following that, the specimens were submerged in deionized water in a supersonic tub for 30 seconds to evacuate propylene glycol, insecurely devoted ZnO, and $Zn(OH)_2$ grains deprived of any responses. Responses are proceeding as follows

$$ZnCl_2 + 2NH_4OH \leftrightarrow Zn(OH)_2 + 2NH^+_4 + 2Cl^-$$

$$Zn(OH)_2 + 4NH4+ \leftrightarrow [(Zn(NH_3)_4]^{2+} + 2H_2O + 2H^+$$
(zinc complex solution $[Zn(NH_3)_4]^{2+}$

$$[Zn(NH_3)_4]^{2+} + 4H_2O \rightarrow Zn(OH) + 4NH^{4+} + 2OH^-$$
(makes $Zn(OH)_2$ solid)

$$Zn(OH)_2 \rightarrow ZnO + H_2O$$ (makes ZnO solid)

Varie cycles were prepared (S5, S10, S15, S20, Si20, and pSi20) for optical investigation, and selected the best cycle for fabricating photodetectors. S5 involved five cycles of ZnO deposition on a glass base, S10 involved ten cycles, S15 involved fifteen cycles, and S20 involved twenty cycles. Two additional samples were prepared, one on a silicon base and the other on a porous silicon surface at a rate of twenty cycles. The one-cycle process and the creation of a zinc composite $[Zn(NH_3)_4]^{2+}$ precursor solution is depicted in figure 1. The thickness of prepared ZnO films was measured by an optical reflectometer system (model: Filmetrics F20). The thicknesses of the films ranged from 450 to 500 nm according to cycles.

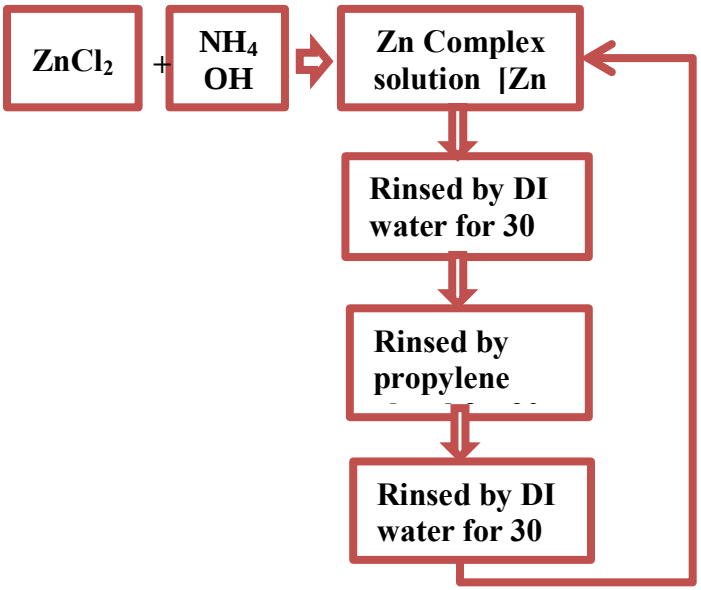

Figure 1: Schematic illustration of formation of ZnO nanostructure using SILAR method.

2.3 Manufacturing photodetectors

Aluminum(Al) metal with (99.99%) purity was deposited using the thermal evaporation unit(model: JEE- 4B/4C) on the front surfaces of ZnO on Si and pSi to create the planar *(ZnO/Si)* and *(ZnO/pSi)* heterojunction photodetectors. The Al grid has been coated by using the metal shadow mask. The grid-metal contact was comprised of five fingers with two interdigitate (electrodes) contacts as shown in figure 1. The dimensions of every figure were 0.7 mm and 5.2 mm in width and length, respectively. The spacing distance between the two fingers was 0.6 mm. The produced photodetector has an active area of about 0.4175 cm^2. The optical properties of samples were examined using an ultraviolet-visible (UV–Vis) Shimadzu-UV 1800 spectrophotometer ranging from(200 nm–1200 nm). To examine the crystal structures of a sample, a radiation source with λ = 1.5406Å wavelength was used with a diffractometer, a Shimadzu (XRD) 6000. Cu (Kα). The morphology and size of pores were studied by FESEM analysis using a field emission scanning electron microscope, FESEM type(JEOLJSM-7900F). Fourier-transform infrared (FTIR) spectra of the ZnO thin films

were measured with an IR prestige-21 FTIR Spectrophotometer, Shimadzu

Current-voltage(I-V)measurements of photodiodes were made at various bias voltages ranging from 0 to 10 V. The Keithley source unit probes (4200 system, Cleveland, United States) were connected to the test fixture to measure the photodetectors' I–V relationship characteristics. For spectra photocurrent measurements, a halogen-tungsten lamp of 100 mW/cm^2 was used as a light source. The monochromator type (MP-1018B) which monitors manually between 100 nm and 1140nm at an interval of 10 nm is used. The intensity of the halogen lamp over the required range was controlled through a current-voltage source.

3. Results and Discussion

3.1 ZnO Optical Characteristic

Figure 2 shows the optical absorbance behavior of ZnO nanostructure layers at an annealing temperature of 400 ℃ on transparency glass as a relationship of wavelength, utilizing UV–Vis spectrophotometer. It demonstrates that the absorbance is increased with deposition cycles from 5 to 20. In the UV–Vis spectrum, the peaks that represent maximum absorption changed depending on the cycle deposition from 5 to 20 cycles. This could be the result of additional band edge absorption that is cycle-dependent. The value of the energy band gap of ZnO thin film can be calculated from Tauc's plot using the relation:

$$(\alpha h\nu) = A\left(h\nu - E_g\right)^n \quad \ldots\ldots\ldots\ldots\ldots (1)$$

Here, the optical band gap is represented by Eg, n=1/2 denotes straight permissible transmission, and A is a constant. The onset absorption is extrapolated to the energy axis (see the inset of Figure 2) to yield the optical band gap Eg. Table (1) has the values of E_g recorded. The results indicated that the sample with 20 cycles had an optical bandgap of 3.39 eV, which is confirmed by (Pon, et al., 2021). This occurs as a result of the ZnO thin film's initial nonuniform surface morphology, which becomes uniform with an increase in cycle count. Doing this propriety, these samples were selected to manufacture the photodetectors.

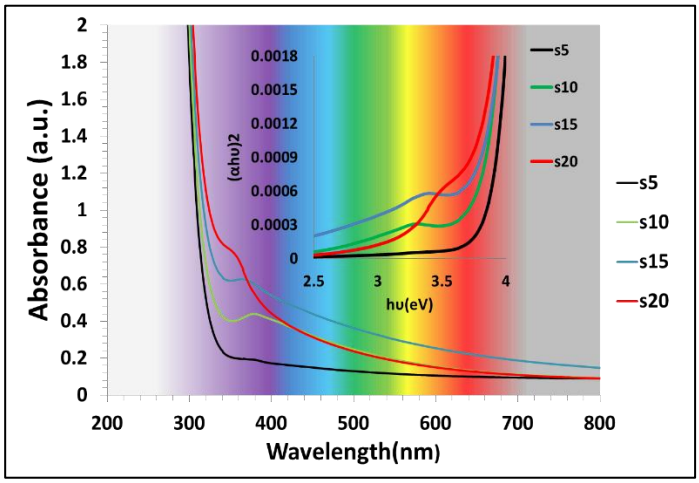

Figure 2: The optical bandgap and absorbance of ZnO nanostructures for various deposition cycles.

Table 1: Optical band gaps of ZnO nanostructures for various number of cycles.

Samples	S5	S10	S15	S20
Energy gap (eV)	3.8	3.68	3.54	3.39

3.2 Structure and Morphology of ZnO

Figure 3 shows the x-ray analyses of diffraction of *(ZnO/Si)* and *(ZnO/pSi)* at a temperature annealing 400℃. The x-ray analyses of diffraction of ZnO grown on porous surfaces *(ZnO/pSi)* are shown in Fig. 3a. The patterns display no characteristic reflection of ZnO peaks clearly due to porous substrate. The broad bands and variations at 69.22° are caused by Si pore surface fluctuations. This is an agreement with (Shabannia, 2015).

Figure 3b shows the x-ray analyses of the diffraction of ZnO on silicon surfaces *(ZnO/Si)*. The reflection peaks at 2θ= 31.8355°, 34.5207°, 36.2871°, 47.5808°, 56.6487°, 62.8917, corresponding to the peak (100), (002), (101), (102), (110) and (103). It was observed that the account for the (002) directed peak's significantly higher intensity than other peaks because the ZnO nanostructure is high (c = 5.2069 Å) oriented and wurtzite crystalline in nature. Every peak corresponds to the Powder Diffraction Standards (JCPDS) card number. 13597-65-4), except a peak that was located at 69.22 which was related to the Si substrates.

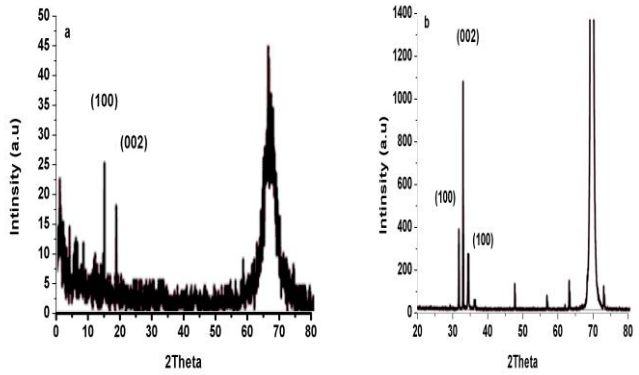

Figure 3: X-ray diffraction of the (a) *(ZnO/pSi)* pattern, and the (b) *(ZnO/Si)* pattern.

Figure 4 shows the field emission scanning electron microscopy surface of the *(ZnO/Si)* and *(ZnO/pSi)* samples. It was found that the diameter of the ZnO nanocrystals was in the range of (20-50 nm) and nearly associated with the characteristics of the surface substrate. The density growth rate of ZnO on the pSi surface is smaller than Si due to the pore surface and some of ZnO has appeared inside the pore if we compare with figure 4b. However, the size of ZnO on each surface (Si and pSi) is the same. This means the surface of substrates is not affected by size ZnO only the rate of growth has been changed. In another way, the silicon substrate causes the particles ZnO to be grouped due to a mismatch between Si and ZnO.

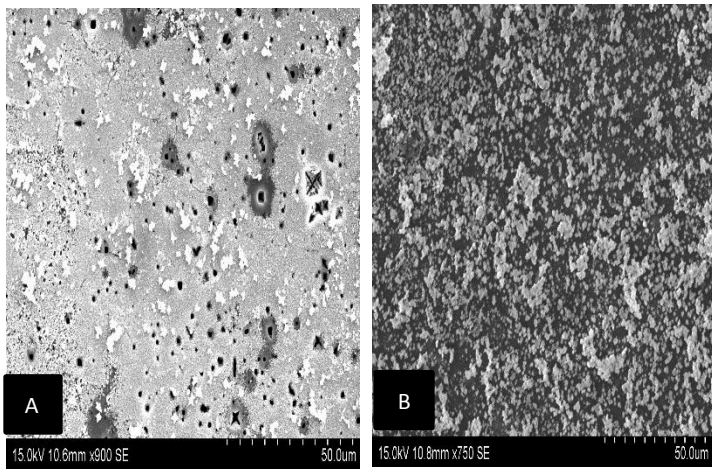

Figure 4: FESEM pictures of (a) *(ZnO/pSi)* and (b) *(ZnO/Si).*

3.3 FTIR Investigation

Figure 5 depicts the FTIR curve of (ZnO/Si) and (ZnO/pSi) fabricated through 15 and 20 cycles and subjected to annealing at a temperature of 400 ℃. Within the spectrum of (ZnO/pSi), the absorption peaks linked to the stretching of Si-O-Si can be observed within the interval of (1109-1106.10 cm-1) of Si-O-Si in the SiOx peaks of pSi is different compared with Si after pore surface by Hf and ethanol the area under the curve of Si-O-Si peak had been larger compared to Si surface due to oxidation during the process. The identification of peaks in the spectral range of 459-460 cm-1 is attributed to an asymmetrical distortion (Kayahan, 2010; Parler, et al., 2001; Singh, et al., 2011). The intensity and the area under the peaks of this symmetric stretch vibration are increased with increasing the number of cycles of deposition. The amplitude and the integral of the peaks of this symmetrical stretching oscillation exhibit an increase as the number of deposition cycles progressively increases.

In contrast, the FTIR curve of *(ZnO/Si)* exhibits notable distinctions compared to that of *(ZnO/pSi)*. The peaks corresponding to Si-O-Si and Si-Si were observed to be significantly diminished, suggesting a reduced level of oxidation and distortion on the silicon surface. Furthermore, the Si-O band appeared to be smaller in magnitude when compared to the porous surface. Notably, a minute peak assigned to the Zn-O band was detected within the range of 459-460 cm-1. This particular band was only observed in the case of ZnO deposition on the porous base, indicating a higher affinity of the porous surface for capturing ZnO particles in comparison to the silicon surface.

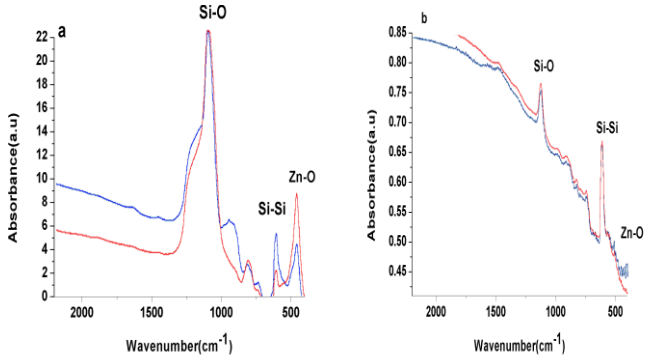

Figure 5: The FTIR curve of (a) *(ZnO/pSi)*, and (b) *(ZnO/Si)* by 15 (red line) and 20 (blue line) cycles.

3.4 I-V Characterization

4. The relationship of current-voltage (I–V) of the planar *(ZnO/pSi)* and *(ZnO/Si)* photodetectors with and without illumination100 mW/cm^{-2} (halogen lamp) is shown in Fig.6. The planar *(ZnO/pSi)* and *(ZnO/Si)* photodetectors consist of two interdigitated Schottky contacts (‘‘fingers’’) deposited on top of the ZnO layer as shown in inset figure 6. The (I–V) curves were measured

using a bias of 0 to 10 V at room temperature. The dark (I–V) curve of the (*ZnO/pSi)* photodetector is different from the *(ZnO/Si)* photodetector. The photodetectors have different dark currents due to the different substrates. As the light reaches the photodetector, the ZnO nanostructure layer captures high-energy photons. Photon-produced charge carriers will be attracted to the metal contacts by fitting the bias voltage, and a photocurrent will be generated. The (I-V) characteristics of the *(ZnO/pSi)* photodetector are shown in figure 6a; this system has a higher forward photocurrent than the *(ZnO/Si)* photodetector since it contains a large surface-to-volume proportion and double heterojunction structures. Furthermore, a noticeable response has been observed at zero bias voltage. Figure 6b depicts the I-V curve of a *(ZnO/Si)* photodetector. In this planar heterojunction package, the current passes through the interface between the Si and ZnO layer at a voltage greater than 3 V, which is due to the nonlinear I-V curve, as shown in comparison(Kayahan, 2010), while in the case of a *(ZnO/pSi)* heterojunction, there is a large forward dark current, which is maybe due to charge carriers moving through the porous layer and layer interfaces.

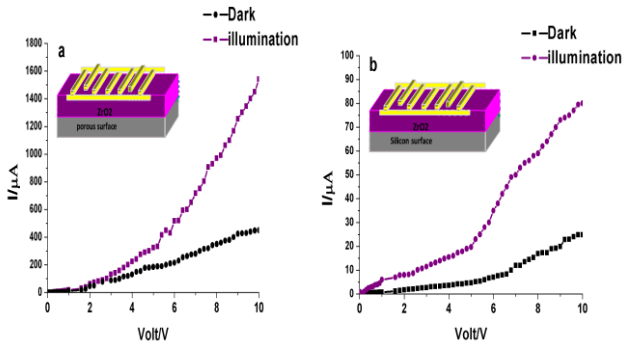

Figure 6: The relationship (I-V) of (a) *(ZnO/ pSi)*, and (b) *(ZnO /Si)* photodetectors at(forward bias voltage).

The photocurrent spectrum for *(ZnO/pSi)* and *(ZnO/Si)* photodetectors in the range (300-800 nm) wavelength are shown in Fig.7. The photocurrent spectral characteristics of both photodetectors were measured at 5 V bias voltage. The photocurrent (I_{ph})of each wavelength is equal to $I\text{-}I_{dark}$, where I is a combination of photocurrent and dark current. In this spectrum under the UV light, the observed photocurrent has resulted from the generation of electrons in the ZnO layer so at 400 nm the current drops sharply due to heterojunctions between ZnO and Si, pSi also the photocurrent of *(ZnO/pSi)* is greater than *(ZnO/Si)*. The best performance of each detector is the response to UV and visible light. The response of visible light of both lights with photon energy greater than the band-gap value is absorbed by the silicon and porous silicon, the photocarriers are excited through the metal-semiconductor-metal junction, giving rise to a change in electrical conductivity.

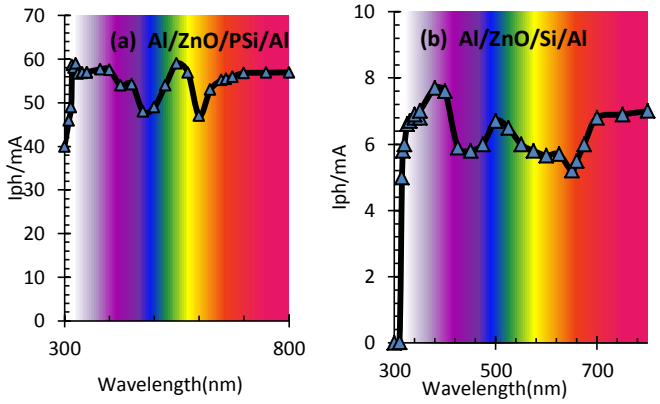

Figure 7: Photocurrent Spectral of planar (a) *(ZnO/pSi)*, and (b) *(ZnO/Si)* photodetector at 5 volts.

Table 2 displays the Responsivity of the (ZnO/pSi) and (ZnO/Si) under varying applied bias voltages of 1 5, and 10 Volts. The responsivity (R) is given by the ratio of photocurrent (Iph) to incident photon power (Pin). (Lan, et al.,2015).

$$R(\lambda) = \frac{I_{ph}}{P_{in}} \ldots\ldots\ldots\ldots (2)$$

Where (I_{ph}) was the generated photocurrent (in mA) equal to $I_{ph} = I_{light} - I_{gark}$ and Pin was the input power of the Halogen-Tungsten light (in Watt). The results stated that the responsivity of ZnO/Porous silicon photodetector is higher than ZnO/silicon. At low voltage, it is equal to 10.833 A/W and 3.607 A/W respectively. At high voltage (Voltage = 10 V) the responsivity is equal to 46.583 A/W for *(ZnO/pSi)* and 23.111 A/W for *(ZnO/Si).* The device reported in this article is better than the previously reported photodetectors (Mohammad, et al., 2015; Al-Hardan, et al., 2015; Shaikh, et al.,2016; Lam, et al.,2017).

Table 2: The Sensitivity and Responsivity of *(ZnO/pSi* and *(ZnO/Si)* (prepared by 20 cycles).

Devices	Voltage (V)	Sensitivity%	R (A/W)	Ref.
ZnO/porous silicon	1	666.66	10.833	This work
ZnO/porous silicon	5	75	3.888	This work
ZnO/porous silicon	10	222	46.583	This work
ZnO/ silicon	1	483	3.607	This work
ZnO/ silicon	5	305	16.278	This work
ZnO/ silicon	10	223	23.111	This work
ZnO/Au/ZnO	1	71.4	2.5 A/W	(Mohammad, et al., 2015)
P-NiO:ZnO/Al:ZnO	5	1834	5.4 A/W	(Al-Hardan, et al., 2015)
ZnO Nanorodes/Cds	5	140	3.83 A/W	(Lam, et al., 2017)
Al/ZnO:ITO NW/Al	5	-	28.2 A/W	(Shaikh, et al., 2016)

The sensitivity (S) is defined as the ratio of photocurrent and dark current, as expressed in Eq. 3 below (Naderi, and Hashim, 2013)

$$S(\%) = \frac{I_{ph} - I_{dark}}{I_{dark}} \times 100 \dots\dots\dots\dots\dots (3)$$

Where I_{dark} is the sample current in the dark, and I_{ph} is the sample current when the sensor is exposed to light. The sensitivity of photodetectors was determined by using Eq.3. Figure 8 shows the photodetector's sensitivity of *(ZnO/pSi)* and *(ZnO/Si)* by varying the bias voltage within the range of 0-10V under illumination. It is evident that as the bias voltage is raised, the photodetectors' sensitivity decreases. As the planar is mounted on a silicon base, it has a sensitivity of 680 % due to a small dark current and high dark conductivity, compared to a low voltage for *(ZnO/pSi)* equal to 270 %. Table (2) indicates the highest sensitivity at 5 V, which was compared to another comparison (Lam, et al., 2017).

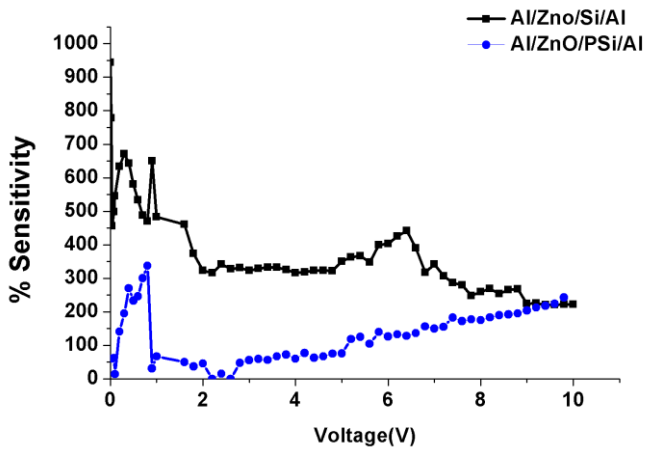

Figure 8: The photodetector sensitivity of *(ZnO/pSi)*, and (*ZnO/Si)* as a varying of bias voltage.

5. Conclusion

The thin film ZnO nanostructure was successfully developed on the pSi, Si, and glass substrates using the SILAR method at various substrate deposition cycles. The investigation focused on studying the impact of varying precipitation cycles on the morphology and optical characteristics of thin ZnO nanostructures. The optical band gap improved with the number of deposition cycles. The XRD measurements showed that a preferential orientation in the (002) direction, with a minimum of ZnO on the Si substrate and no reflection peak, appears of ZnO on pSi due to the pore surface. The nonporous structures play an important role in photodetector characterization, in which larger specific surface areas are a benefit for enhancing responsivity. Therefore, the planar *(ZnO/pSi)* has high responsivity10.833 A/W compared to *(ZnO/Si)* 3.607 A/W, particularly in the long visible wavelengths at low bias voltage, but the sensitivity is opposite at the same voltage. The results evidence that the SILAR technique is a modest, low-priced process for producing high-responsivity and sensitivity photodetectors without the use of complex procedures.

Acknowledgments

The authors express their gratitude for the financial assistance provided by the Ministry of Higher Education of Kurdistan Regine, Iraq, and Salahaddin University. Additionally, they extend their heartfelt appreciation to Dr. Naser Mahmood Ahmed at USM-Malaysia for his invaluable technical guidance.

Financial support: No financial support.

Potential conflicts of interest. All authors report no conflicts of interest relevant to this article.

References

Al Abdullah, K., Awad, S., Zaraket, J. and Salame, C., 2017. Synthesis of ZnO nanopowders by using sol-gel and studying their structural and electrical properties at different temperatures. *Energy Procedia*, *119*, pp.565-570.

Al-Hardan, N.H., Hamid, M.A.A., Ahmed, N.M., Jalar, A., Shamsudin, R., Othman, N.K., Keng, L.K. and Mohammed, S.M., 2015. A study on the UV photoresponse of hydrothermally grown zinc oxide nanorods with different aspect ratios. *IEEE Sensors Journal*, *15*(12), pp.6811-6818.

Al-Heuseen, K., Aljameel, A.I. and Hussein, R.K., 2024. Synthesis and characterization of Cu-Doped ZnO nanostructures for UV sensing application. *BMC Chemistry*, *18*(1), p.32.

Al-Rasheedi, A., Ansari, A.R., Abdeldaim, A.M. and Aida, M.S., 2022. Growth of zinc oxide thin films using different precursor solutions by spray pyrolysis technique. *The European Physical Journal Plus*, *137*(12), pp.1-11.

Bayan, S., 2024. Recent Strategies for Development of ZnO-Based Efficient UV-Photodetectors. In *Nanoscale Matter and Principles for Sensing and Labeling Applications* (pp. 165-179). Singapore: Springer Nature Singapore.

Boruah, B.D., 2019. Zinc oxide ultraviolet photodetectors: rapid progress from conventional to self-powered photodetectors. *Nanoscale Advances*, *1*(6), pp.2059-2085.

Cruz, M.A., Garza-Hernández, R., Horley, P.P., Mata-Ramírez, J., Martínez-G, E. and Aguirre-Tostado, F.S., 2018. Low-temperature ZnO films grown by successive ionic layer adsorption and reaction methods. *Thin Solid Films*, *663*, pp.49-55.

Ghos, B.C., Farhad, S.F.U., Patwary, M.A.M., Majumder, S., Hossain, M.A., Tanvir, N.I., Rahman, M.A., Tanaka, T. and Guo, Q., 2021. Influence of the substrate, process conditions, and post-annealing temperature on the properties of ZnO thin films grown by the successive ionic layer adsorption and reaction method. *ACS omega*, *6*(4), pp.2665-2674.

Govender, K., Boyle, D.S., Kenway, P.B. and O'Brien, P., 2004. Understanding the factors that govern the deposition and morphology of thin films of ZnO from aqueous solution. *Journal of Materials Chemistry*, *14*(16), pp.2575-2591.

Guo, N., Xiao, L., Gong, F., Luo, M., Wang, F., Jia, Y., Chang, H., Liu, J., Li, Q., Wu, Y. and Wang, Y., 2020. Light-Driven WSe2-ZnO Junction Field-Effect Transistors for High-Performance Photodetection. *Advanced Science*, *7*(1), p.1901637.

Jiang, Z., Liu, B., Yu, L., Tong, Y., Yan, M., Zhang, R., Han, W., Hao, Y., Shangguan, L., Zhang, S. and Li, W., 2023. Research progresses in preparation methods and applications of zinc oxide nanoparticles. *Journal of Alloys and Compounds*, p.170316.

Kayahan, E., 2010. White light luminescence from annealed thin ZnO deposited porous silicon. *Journal of Luminescence*, *130*(7), pp.1295-1299.

Khokhra, R., Bharti, B., Lee, H.N. and Kumar, R., 2017. Visible and UV photo-detection in ZnO nanostructured thin films via simple tuning of the solution method. *Scientific reports*, *7*(1), p.15032.

Lam, K.T., Hsiao, Y.J., Ji, L.W., Fang, T.H., Hsiao, K.H. and Chu, T.T., 2017. High-sensitive ultraviolet photodetectors based on ZnO nanorods/CdS heterostructures. *Nanoscale research letters*, *12*, pp.1-7.

Lan, C., Li, C., Yin, Y., Guo, H. and Wang, S., 2015. Synthesis of single-crystalline GeS nanoribbons for high-sensitivity visible-light photodetectors. *Journal of Materials Chemistry C*, *3*(31), pp.8074-8079.

Lu, Y.J., Shi, Z.F., Shan, C.X. and Shen, D.Z., 2019. ZnO nanostructures and lasers. In *Nanoscale Semiconductor Lasers* (pp. 75-108). Elsevier.

Mohammad, S.M., Hassan, Z., Ahmed, N.M., Al-Hardan, N.H. and Bououdina, M., 2015. Fabrication of low-cost UV photodetector using ZnO nanorods grown onto nylon substrate. *Journal of Materials Science: Materials in Electronics*, *26*, pp.1322-1331.

More, P.B., Bansode, S.B., Aleks, M. and Pathan, H.M., 2023. Synthesis of ZnO thin films using chemical bath and investigation of physicochemical properties. *ES Energy & Environment*, *22*, p.983.

Naderi, N. and Hashim, M.R., 2013. Porous-shaped silicon carbide ultraviolet photodetectors on porous silicon substrates. *Journal of Alloys and Compounds*, *552*, pp.356-362.

Nikov, R.G., Dikovska, A.O., Nedyalkov, N.N., Atanasov, P.A., Atanasova, G., Hirsch, D. and Rauschenbach, B., 2017. ZnO nanostructures produced by pulsed laser deposition in open air. *Applied Physics A*, *123*, pp.1-7.

Parler, C.M., Ritter, J.A. and Amiridis, M.D., 2001. Infrared spectroscopic study of sol-gel derived mixed-metal oxides. *Journal of non-crystalline solids*, *279*(2-3), pp.119-125.

Pon, V.D., Wilson, K.J., Hariprasad, K., Ganesh, V., Ali, H.E., Algarni, H. and Yahia, I.S., 2021. Enhancement of optoelectronic properties of ZnO thin films by Al doping for photodetector applications. *Superlattices and Microstructures*, *151*, p.106790.

Rahman, F., 2019. Zinc oxide light-emitting diodes: a review. *Optical Engineering*, *58*(1), pp.010901-010901.

Rahman, M.A., Mamun, S.N., Hossain, A.K.M.A. and Ton-That, C., 2023. ZnO Nanorods on Li-Doped ZnO Thin Films for Efficient p–n Homojunction Light-Emitting Diodes. *ACS Applied Nano Materials*, *6*(17), pp.15757-15763.

Shabannia, R. and Naderi, N., 2019. Effect of growth time on ZnO thin films prepared by low-temperature

chemical bath deposition on PS substrate. *Journal of Nanoanalysis*, *6*(2), pp.99-104.

Shabannia, R., 2015. Vertically aligned ZnO nanorods on porous silicon substrates: Effect of growth time. *Progress in Natural Science: Materials International*, *25*(2), pp.95-100.

Shaikh, S.K., Inamdar, S.I., Ganbavle, V.V. and Rajpure, K.Y., 2016. Chemical bath deposited ZnO thin film-based UV photoconductive detector. *Journal of Alloys and Compounds*, *664*, pp.242-249.

Shaoqiang, C., Ziqiang, Z., Jianzhong, Z., Jian, Z., Yanling, S., Ke, Y., Weiming, W., Xiaohua, W., Xiao, F., Laiqiang, L. and Li, S., 2004. Hydroxyapatite coating on porous silicon substrate obtained by precipitation process. *Applied Surface Science*, *230*(1-4), pp.418-424.

Singh, R.G., Singh, F., Mehra, R.M., Kanjilal, D. and Agarwal, V., 2011. Synthesis of nanocrystalline α-Zn2SiO4 at ZnO–porous silicon interface: Phase transition study. *Solid State Communications*, *151*(9), pp.701-703.

Sreedev, P., Rakhesh, V., Roshima, N.S. and Shankar, B., 2019, March. Preparation of Zinc Oxide Thin Films by SILAR method and its Optical analysis. In *Journal of Physics: Conference Series* (Vol. 1172, No. 1, p. 012024). IOP Publishing.

Syrek, K., Tynkevych, O., Wojtas, M., Kozieł, M., Pięta, Ł. and Zaraska, L., 2023. Room-temperature electrochemical deposition of nanostructured ZnO films on FTO substrate and their photoelectrochemical activity. *Journal of Industrial and Engineering Chemistry*, *126*, pp.171-180.

Tripathy, A., Wąsik, P., Sreedharan, S., Nandi, D., Bikondoa, O., Su, B., Sen, P. and Briscoe, W.H., 2018. Facile fabrication of multifunctional ZnO urchins on surfaces. *Colloids and Interfaces*, *2*(4), p.74.

Wang, P., Jin, C., Wu, X., Zhan, H., Zhou, Y., Wang, H. and Kang, J., 2012. Quality improvement of ZnO thin layers overgrown on Si (100) substrates at room temperature by nitridation pretreatment. *AIP Advances*, *2*(2).

Wisz, G., Virt, I., Sagan, P., Potera, P. and Yavorskyi, R., 2017. Structural, optical, and electrical properties of zinc oxide layers produced by pulsed laser deposition method. *Nanoscale Research Letters*, *12*, pp.1-7.

Xu, L., Li, X., Zhan, Z., Wang, L., Feng, S., Chai, X., Lu, W., Shen, J., Weng, Z. and Sun, J., 2015. Catalyst-free, selective growth of ZnO nanowires on SiO2 by chemical vapor deposition for transfer-free fabrication of UV photodetectors. *ACS Applied Materials & interfaces*, *7*(36), pp.20264-20271.

Zhang, Y., Ji, T., Zou, R., Ha, E., Hu, X., Cui, Z., Xu, C., Xu, K., Zhang, Y. and Hu, J., 2020. An efficiently enhanced UV-visible light photodetector with a Zn: NiO/p-Si isotype heterojunction. *Journal of Materials Chemistry C*, *8*(10), pp.3498-3508.